

Article

Synthesis and Characterization of Ni–W/Cr₂O₃ Nanocomposite Coatings Using Electrochemical Deposition Technique

Samuel Mbugua Nyambura ¹, Min Kang ^{1,2,*} , Jiping Zhu ³, Yuntong Liu ¹, Yin Zhang ¹ and Ndumia Joseph Ndiithi ¹ 

¹ College of Engineering, Nanjing Agricultural University, Nanjing 210031, China; accessmbugua@gmail.com (S.M.N.); 2017112003@njau.edu.cn (Y.L.); 2018212003@njau.edu (Y.Z.); 2017112122@njau.edu.cn (N.J.N.)

² Guanyun Research Institute for Modern Agricultural Equipment, Nanjing Agricultural University, Guanyun 222200, China

³ Ministry of Agriculture and Rural Affairs, Nanjing Research Institute for Agricultural Mechanization, Nanjing 210000, China; zhujip@163.com

* Correspondence: kangmin@njau.edu.cn; Tel.: +86-25-5860-6667

Received: 21 October 2019; Accepted: 28 November 2019; Published: 2 December 2019



Abstract: Ni–W/Cr₂O₃ nanocomposite coatings were synthesized from aqueous sulphate-citrate electrolyte containing Cr₂O₃ nanoparticles on a steel surface using conventional electrodeposition technique. This study was aimed at investigating the influence of Cr₂O₃ nanoparticle content on the microstructure, corrosion resistance, and mechanical properties of electrodeposited Ni–W/Cr₂O₃ nanocomposite coatings. Ni–W binary alloy coatings were deposited and optimized before addition of the nanoparticles to produce high-quality coatings. The microstructure and chemical composition of the Ni–W/Cr₂O₃ nanocomposite coatings were evaluated using scanning electron microscope (SEM), energy dispersive X-ray spectrometer (EDS), and XRD. Corrosion resistance properties were evaluated using potentiodynamic polarization (Tafel) measurements in 3.5 wt.% NaCl medium. The corrosion resistance and microhardness are significantly higher in Ni–W/Cr₂O₃ nanocomposite coatings compared to pure Ni–W binary alloy and increase with the increase in content of Cr₂O₃ nanoparticles in the coatings. Wear resistance is also higher in Ni–W/Cr₂O₃ nanocomposite coatings.

Keywords: nanocomposite coatings; conventional electrodeposition; corrosion resistance; microhardness; wear resistance

1. Introduction

Material surfaces form one of the key pillars in engineering. However, surfaces are under constant threat of corrosion and wear, which increases maintenance costs and decreases operating efficiency in industry. Over the years, research has been done on surface modification technologies to mitigate wear and corrosion of materials, or prevent them altogether has become an obvious necessity [1]. There has been an increase in the demand and interest in composite materials development with precisely controlled properties. Metal matrix composites (MMCs) are comprised of matrices whose phases are made up of either metal or metal alloy and reinforcements, which can range from carbide, nitride, ceramic, oxide, to metallic particles. Such MMCs find wide use in automobile and aerospace industries owing to their excellent isotropic, physical, and chemical properties [2]. Many techniques for synthesis of MMC coatings have been devised. These include nitridation, powder metallurgy, hard facing, electrochemical deposition, plasma spraying, thermal spraying, pressureless infiltration, chemical vapour deposition, and casting techniques [3,4].

Electrodeposition is one of the most widely used coating techniques owing to its simplicity, rapid deposition rates, and cost effectiveness [5]. Electrodeposited composites are comprised of two phases, the highest volume fraction solid phase, termed the matrix, and the reinforcement. The matrix phase consists of alloys, which can be binary, ternary, or quaternary depending on the number of metals used to form the alloy. Electrodeposition can be used to synthesize uniform metallic, alloy, and metallic matrix coating with a wide range of coating thicknesses and specific characteristics in either single layers or multiple layers [6]. Electrodeposition also offers the unique possibility to synthesize nanocomposite coatings, which often exhibit superior properties in comparison to traditional grain-sized materials [7]. Electrodeposited nanocomposite coatings allow for more favourable properties compared to purely metallic coatings or alloy coatings because the inherent properties of the reinforcement nanoparticles further improve the overall properties of the nanocomposite coatings.

During electrodeposition, the suspended nanoparticles become engulfed in an ionic cloud after which they are transferred toward the cathode as a justification of the following theories: Electrophoresis force, mechanical entrapment, adsorption, and convective diffusion. The nanoparticles are then diffused into the cathode surface via a hydrodynamic boundary layer followed by consecutive diffusion through a concentrated boundary layer. The nanoparticles then become entrapped on the cathode where they become embedded into the growing matrix coating [8]. These innovative materials possess endless application possibilities since their properties can be tailored accurately through choice of dispersive phase and the matrix to suit specific applications.

In recent years, W alloys have attracted a lot of interest owing to their unique and excellent properties; that is, high hardness (as well as hot hardness), low coefficient of thermal expansion, high melting point, high tensile strength, high wear resistance, and good corrosion resistance [9–11]. W cannot be electrodeposited alone but can be readily deposited with iron group metals such as Ni in a process called induced codeposition [12]. Ni–W alloys have drawn a lot of interest as a substitute for hard chromium coatings whose electrolytic baths contain toxic hexavalent chromium that is harmful to the environment [13,14]. Research shows that using induced codeposition, amorphous Ni–W can be electrodeposited, which results in improved corrosion resistance of substrate surfaces [12,15]. Donten et al. [16] researched on three tungsten alloys (Fe–W, Co–W, Ni–W) and found that electrodeposited amorphous Ni–W alloy exhibits the best smoothness and appearance, but has poor adhesion properties on the steel substrates. Also, the alloy has high internal stresses that cause formation and propagation of micro-cracks in the alloy matrix [16]. Yamasaki et al. [17] reported that increase in W content in the coating led to an overall increase in wear resistance, but this in turn increased surface cracking of the Ni–W coatings. Other electrodeposited W alloys include Ni–Fe–W, Fe–Cr–W, Ni–W–Fe, and Ni–W–Cu–P. Although these alloy coatings exhibit superior corrosion and wear resistance, the constant need for better materials has led researchers to embed various nanoparticles in the Ni–W alloy matrix as the reinforcement. The electrodeposited Ni–W nanocomposite coatings have been found to exhibit far superior resistance to corrosion and wear compared to purely Ni–W binary alloys. Research done on electrodeposited Ni–W/SiC nanocomposite coatings reported that hardness and modulus of the nanocomposite coatings increased with increase in the content of SiC [18]. Research also showed that the Ni–W/ZrO₂ nanocomposite coatings exhibited considerably better microhardness than Ni–W coatings [19]. Other nanoparticles that have been electrodeposited with Ni–W alloy include Al₂O₃, TiO₂, and SiO₂. The authors of [20] investigated the contribution of Cr₂O₃ nanoparticles on the mechanical and corrosion properties of Ni–Co alloy. It was found that Cr₂O₃ nanoparticles drastically improved Ni–Co microhardness as a consequence of three factors: Alteration of the microstructural heterogeneity by providing favourable locations for heterogenous Co particle nucleation, inherent hardness of the Cr₂O₃ nanoparticle, and filling of micro-cracks on the coating structure. Also, an improvement in corrosion resistance was reported with incorporation of Cr₂O₃ nanoparticles as a result of the combined increase in both Cr₂O₃ and Co in the Ni–Co nanocomposite coatings. Zhang et al. [21] electrodeposited Ni–W/Cr₂O₃ with a constant current density of 4 A·dm^{−2}. However, research on the

wear properties of electrodeposited Ni–W/Cr₂O₃ has not been done. Similarly, the effect of current density on electrodeposited Ni–W/Cr₂O₃ nanocomposites has not been researched.

This study is aimed at investigating the wear resistance of Ni–W/Cr₂O₃ nanocomposite coatings as well as the effect of varying electrodeposition parameters on the microstructure and corrosion characteristics of electrodeposited Ni–W nanocrystalline coatings reinforced with Cr₂O₃ nanoparticles using conventional electro-deposition (CECD) technique. The present study focuses on the effect of electrodeposition conditions on the electrodeposited Ni–W/Cr₂O₃ nanocomposite coatings in order to determine the optimum fabrication conditions. The mechanical and microstructural characteristics on electrodeposited Ni–W/Cr₂O₃ from the subsequent fabrication conditions were also analysed.

2. Experiment

2.1. Preparation of Ni–W/Cr₂O₃ Nanocomposite Coatings

The Ni–W alloy coatings embedded with Cr₂O₃ nanoparticles were electrodeposited from aqueous sulphate–citrate solution using conventional electrodeposition technique in a modified watts bath with varying concentrations of Cr₂O₃. Steel A103 samples measuring 30 mm × 8 mm × 7 mm were used as the substrate material to provide suitable substrate surfaces for electrodeposition and a pure nickel plate measuring 150 mm × 50 mm × 2 mm was used as the anode. The anode was chosen such that it had a surface area much larger than that of the substrate to prevent anodic polarization of the Ni plate. So as to provide good surfaces for electrodeposition, the steel substrates were mechanically polished using 300–2000 abrasive emery paper (silicon carbide) prior to electrodeposition.

Steel A103 substrates usually require a pre-treatment sequence to ensure quality deposits. The samples were pre-treated using a triple immersion procedure for electric cleaning so as to create a stronger bond between the substrate and the coatings. First, the samples were cleaned using the electro-hydrostatic fluid to degrease them. Secondly, the samples were passed through a strong activating solution to remove any oxide layer on the surface. Lastly, the samples were treated using a weak activating solution to remove carbon-black on the surface. Deionized water was used to rinse the substrate samples after each pre-treatment step. The individual reagents of the alkali-based degreasing solution and the HCl pickling solutions used in pre-treatment and their concentrations are listed in Table 1.

Table 1. Pre-treatment process of substrate surface.

Process	Fluid Type	Chemical Composition	Concentration (g·L ⁻¹)
Degreasing	Electro-hydrostatic fluid	NaOH	25
		Na ₂ CO ₃	21.7
		NaPO ₄	50
		NaCl	2.4
Pickling	Activating fluid 1	HCl	25
		NaCl	140.1
	Activating fluid 2	Na ₂ C ₂ O ₄ ·2H ₂ O	141.2
		H ₃ C ₆ H ₅ O ₇ ·H ₂ O	94.2
		NiCl ₂ ·H ₂ O	3

After pre-treatment was concluded, the samples were rinsed using distilled water and immediately immersed into the electrolyte solution. The electrolyte solution consisted of analytical grade reagents and deionized water. The electrolyte compositions, purpose of each component is shown in Table 2. The electrodeposition parameters for the experiment are shown in Table 3. The Cr₂O₃ used in the experiment were 99 wt.% pure and had an average diameter of 20 nm. The Cr₂O₃ nanoparticles were added into the electrolyte and the solution was vigorously stirred at 700 rpm for 24 h to keep the Cr₂O₃ nanoparticles in suspension. Particle agglomeration in the matrix significantly degrades the mechanical properties of the electrodeposited nanocomposite coatings. Hence, a critical objective

in electrodeposition of Ni–W–Cr₂O₃ nanocomposite coatings is achieving stable and homogeneous Cr₂O₃ nanoparticle dispersion in electrolyte using additives. Sodium dodecyl sulphate was added in the electrolyte solution to maintain surface charge adjustment, ensure better nanoparticle dispersion, and also to prevent particle agglomeration.

Table 2. Chemical composition of main citrate–sulphate electrolyte bath.

Bath Component	Concentration (g·L ⁻¹)	Function
Nickel sulphate (NiSO ₄ ·7H ₂ O)	250	Ni source
Nickel chloride (NiCl ₂ ·6H ₂ O)	50	Ni source
Sodium tungstate (Na ₂ WO ₄ ·2H ₂ O)	10, 20, 30, 40	W source
Trisodium citrate dihydrate (Na ₃ C ₆ H ₅ O ₇ ·2H ₂ O)	90	Complexer for Ni and W
Boric acid (HBO ₃)	40	Buffer
Potassium bromide (KBr)	15	Conductivity increase
Sodium saccharin (COC ₆ H ₄ SO ₂ NNa·2H ₂ O)	1	Stress reliever
Sodium dodecyl sulphate (SDS)	0.5	Surfactant
Cr ₂ O ₃ (20 nm)	0, 2, 6, 10, 20	Nanoparticles

Table 3. Electrodeposition parameters.

Deposition Parameters						
Plating Temperature (°C)	Current Density (A·dm ⁻²)	Stirring Rate (rpm)	pH	Electrodeposition Time (min)	Current Type	Anode Material
45	1, 2, 3	350	5.5 ± 0.2	60	DC	Pure Ni (99%)

The electrodes were placed vertically 3 cm apart in a 1 L beaker of electrolyte solution. A magnetic stirrer was used to agitate the electrolyte with a stirring speed of 350 rpm to prevent agglomeration of nanoparticles, thereby ensuring homogeneity of the electrodeposited coatings. The electrolyte temperature was maintained at 45 °C throughout the entire experiment. A deposition time of 1 h was chosen for all the samples to ensure a uniform thickness of the electrodeposited coating. After the electrodeposition process, double distilled water was used to clean the electrodeposited coatings ultrasonically for 10 min to dislodge the loosely embedded Cr₂O₃ nanoparticles from the substrate surface. To synthesize the Ni–W/Cr₂O₃ nanocomposite coatings with the best microhardness and corrosion resistance properties, Ni–W coatings were first synthesized and optimized by varying the W content in the coatings. The coatings that exhibited the best properties was then selected for embedding with the Cr₂O₃ nanoparticles. For comparison purposes, Ni–W coatings were electrodeposited under the same parameters without adding the Cr₂O₃ nanoparticles into the electrolytic cell solution.

2.2. Surface Morphology and Phase Determination

The microstructure and surface morphologies of the electrodeposited coatings were studied using FEI Quanta FEG 250 scanning electron microscope (SEM, Hillsboro, OR, USA). Energy dispersive spectrometer (EDS Oxford max 20, Abingdon, UK) coupled with SEM was used to investigate the individual element composition, chemical analysis, and content of the coatings. The average grain size, phase structure, and preferred orientation of the electrodeposited coatings were analyzed using X'Pert Power X-ray diffraction (XRD, Westborough, MA, USA). In this analysis, crystallite size of the deposits was determined using integral peak width. The average particle size of the deposited coatings was determined using the Debye–Scherrer formula shown in Equation (1) [22]:

$$D = \frac{k\lambda}{\beta \cos\theta'} \quad (1)$$

where D represents the average crystallite size (nm), k represents the Scherrer constant, λ the X-ray wavelength (1.5406), β the full width at half maximum (rad), and θ the Bragg angle.

The microhardness of the deposits was measured using Vickers microhardness tester using a load of 200 g and an indentation time of 10 s for each loading. An average of 10 separate location measurements on each sample surface was taken as the microhardness of the electrodeposited coatings. The wear test was done using a high-frequency reciprocating wear test machine with a ball on disk pair. Before and after each test, the samples were ultrasonically cleaned in acetone. No lubrication was used in the friction and wear test. The surface morphologies showing the worn grooves were analyzed using scanning electron microscope.

Current efficiency was calculated using the weight of the deposits which was given by the difference between the weight of the samples before and after the electrodeposition process. This is shown in Equation (2) [23]:

$$\eta = W/It \sum (Fge)/KN \times 100, \quad (2)$$

where η is the current efficiency (%), W the deposited coating weight (g), I represents the current (A), t is the time (h), F the Faraday constant (96,485.3 C/mol), g the element weight fraction in the deposit (Ni or W), e the number of electrons needed to reduce 1 mol atoms of Ni and W ($e = 2$ for Ni, $e = 6$ for W), K represents a unit conversion factor (3600 C/A h), and N is the element atomic weight (Ni = 58.693 g/mol, W = 183.84 g/mol). An assumption was held that the incorporated Cr₂O₃ nanoparticles did not affect the validity of the results.

The corrosion resistance of the coatings was analyzed using potentiodynamic polarization measurements. The potentiodynamic polarization of the electrodeposited coatings was analyzed using a potentiodynamic scanning system. An electrochemical workstation containing 3.5 wt.% NaCl corrosive medium was used to carry out all the electrochemical measurements without agitation. The polarization resistance (R_p), corrosion potential (E_{corr}), and corrosion current density (i_{corr}) were analyzed using Tafel extrapolation method. A saturated calomel electrode (SCE) was used as the reference electrode. The samples were first immersed into the corrosive medium to attain open circuit potential (E_{ocp}) after which potentiodynamic sweeping was immediately undertaken with a potential range of 600 mV for both the alloy coating and nanocomposite coating with respect to E_{ocp} using 1.0 mV/s sweep rate. The Stern–Geary equation was used to determine the polarization resistance from the polarization measurements. This is represented in Equation (3) [24]:

$$R_p = \frac{\beta_a \times \beta_c}{2.303 \times i_{corr}(\beta_a + \beta_c)}, \quad (3)$$

where R_p represents the polarization resistance, i_{corr} represents the corrosion current density of the coatings, and β_a and β_c represent the anodic and cathodic Tafel slopes, respectively.

3. Results

3.1. Ni–W Alloy Coatings

3.1.1. W Content

It can be seen from Figure 1 that the Ni and W elements were successfully deposited in the coatings.

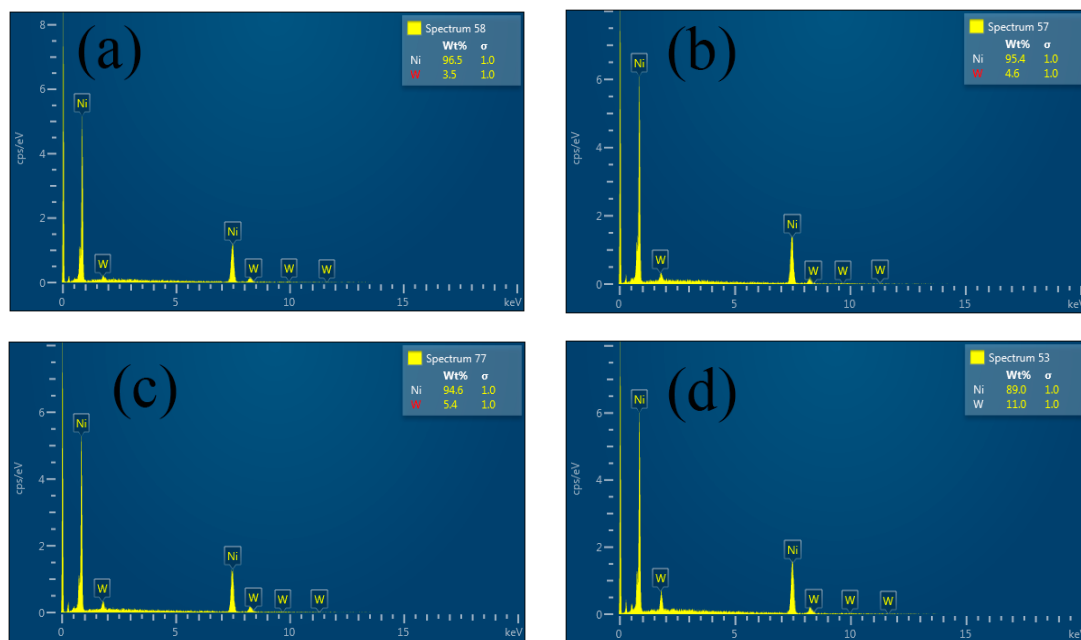


Figure 1. EDS spectra of Ni–W nanocomposite coatings electrodeposited at (a) 10, (b) 20, (c) 30, and (d) 40 g·L⁻¹ W ($i_d = 1 \text{ A}\cdot\text{dm}^{-2}$).

The W content had an obvious increasing trend from 3.5 wt.% at 10 g·L⁻¹ to a maximum of 11.0 wt.% at 40 g·L⁻¹. Brener, A. The authors of [25] classified this phenomenon as induced codeposition, where the reluctant element is W and Ni is the inducing metal. The explanation to this phenomenon is still somewhat uncertain. It has been suggested, however, that in Ni–W binary alloy electrodeposition, the precursor reaction is presumed to be the complex $[(\text{Ni})(\text{WO}_4)(\text{H})(\text{Cit})]^{2-}$ derived from Equation (4) [26]:



Although the reaction postulates that the alloy contains a single atom of Ni and a single atom of W, it is highly unlikely to achieve a Ni–W alloy of the ratio 1:1. This is attributed to several concurrent reactions that result in the deposition of Ni metal against a single or two reactions leading to deposition of Ni and W in a ratio of 1:1. Ni forms complexes with NH₃ and citrates, but W can only be deposited from mixed-metal complexes [26,27].

3.1.2. Corrosion Resistance

Figure 2 shows the potentiodynamic polarization curves of Ni–W alloy deposited with varying concentrations of W in the electrolyte ranging from 10, 20, 30, to 40 g·L⁻¹ at 1 A·dm⁻².

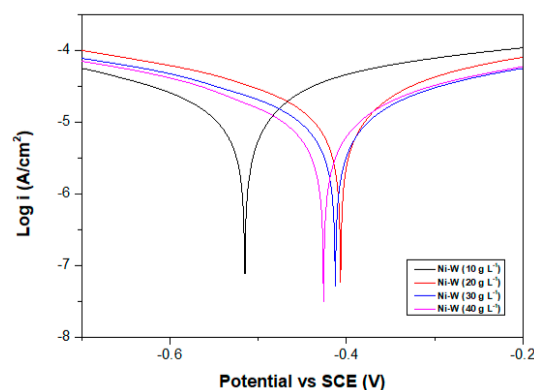


Figure 2. Potentiodynamic polarization curves for Ni–W with varying contents of W in the coatings.

Table 4 summarizes the electrochemical data collected from the potentiodynamic polarization curves.

Table 4. Potentiodynamic polarization measurements of Ni–W nanocomposite coatings with varying contents of W ($i_d = 1 \text{ A}\cdot\text{dm}^{-2}$).

Coatings	β_a (mV)	β_c (mV)	E_{corr} (mV)	i_{corr} ($\mu\text{A}\cdot\text{cm}^{-2}$)	Corrosion Rate (mm/a)	R_p ($\text{k}\Omega\cdot\text{cm}^{-2}$)
Ni-3.5W	414.38	780.15	−515	39.639	0.479	2.964
Ni-4.6W	409.04	659.58	−406	37.392	0.452	2.931
Ni-5.4W	482.54	649.65	−412	29.648	0.358	4.055
Ni-11.0W	395.48	545.57	−426	22.461	0.271	4.432

It can be seen that the highest polarization resistance coupled with the lowest corrosion current density corresponded to the Ni–W alloy coatings that contained 11.0 wt.% W. It can therefore be stated that the lowest corrosion rate of Ni–W binary alloy coatings was exhibited by Ni–11.0W alloy coatings. Increase in corrosion resistance with increase in W content of the Ni–W binary alloy coatings may be attributed to chemical composition and crystallite size. The nobility of Ni and W is changed when the binary alloy is formed and this change influences the corrosion resistance of the resulting coatings [28].

Table 5 shows the grain sizes of Ni–W binary coatings as a function of increasing W content in the coatings. Grain sizes of the Ni–W binary alloys were derived from integral width of XRD (Ni 111) index planes using the Scherrer equation. From the results, it can be seen that the grain sizes of the Ni–W binary alloy coatings decreased from 163.58 nm in Ni-3.5W to 111.59 nm in Ni-11.0W. This decrease in grain size can be attributed to formation of Ni hydroxides in the plating bath, which can act as grain refiners, block, or be adsorbed into the active growth centers [29]. From the corrosion measurements, it can be seen that corrosion resistance of Ni–W binary alloys increased with increase in W concentration in the electrolyte and this can be attributed to solid solution strengthening where Ni and W elements combine to form a solid solution matrix. Other factors that may factor into the change in corrosive resistance of the Ni–W binary coatings include preferred orientation and phase structure.

Table 5. Grain sizes of Ni–W binary coatings as a function of Scherrer’s equation.

Coatings	W Concentration ($\text{g}\cdot\text{L}^{-1}$)	W Content (wt.%)	Grain Size (nm)
Ni–W	10	3.5	163.5
Ni–W	20	4.6	149.9
Ni–W	30	5.4	164.5
Ni–W	40	11.0	111.5

3.2. Ni–W–Cr₂O₃

3.2.1. SEM

SEM images of pure Ni–W binary alloy coatings were analyzed for comparison purposes and are displayed in Figure 3a–d. In all the Ni–W coatings, it was observed that coatings with high W content (11.0 wt.%) developed micro-cracks. Similar observations were found by Allahyarzadeh et al. [30]. This could be attributed to conducting experiments with direct current and utilizing only one complexing agent, which resulted in crack formation on surface of the electroplated binary alloy [13]. Also, the cracking phenomena is as a result of good adhesion between the substrate and coating where high stresses are released by crack generation and propagation [13,31]. To illustrate the influence of Cr₂O₃ nanoparticle concentration on the surface morphology of Ni–W/Cr₂O₃ nanocomposite coatings, SEM images were analyzed as shown in Figure 4a–d. From Figure 4a–d, it is evident that the surface morphology is significantly influenced by the concentration of Cr₂O₃ nanoparticles in the plating solution. The Ni–W/Cr₂O₃ composite coatings formed with $2 \text{ g}\cdot\text{L}^{-1}$ Cr₂O₃ were nodular in nature. Increased Cr₂O₃ concentration to $6 \text{ g}\cdot\text{L}^{-1}$ and $10 \text{ g}\cdot\text{L}^{-1}$ produces elliptical clusters on the coatings surface, which comprise of small globules. At $20 \text{ g}\cdot\text{L}^{-1}$, the coatings display a more amorphous tendency characterized by cavities. Similar observations were reported by Zhang et al. [21].

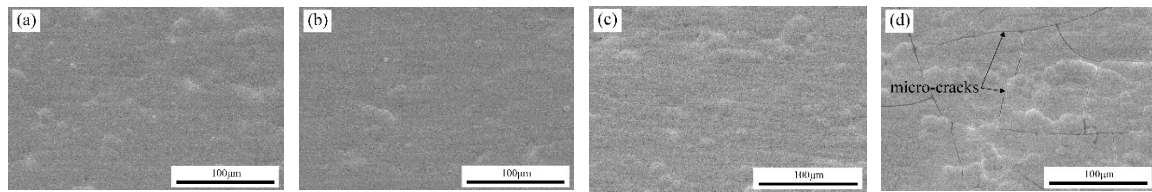


Figure 3. SEM images of the surface morphologies of Ni-W binary alloy coatings deposited at different W concentrations: (a) $10 \text{ g}\cdot\text{L}^{-1}$, (b) $20 \text{ g}\cdot\text{L}^{-1}$, (c) $30 \text{ g}\cdot\text{L}^{-1}$, and (d) $40 \text{ g}\cdot\text{L}^{-1}$ ($i_d = 1 \text{ A}\cdot\text{dm}^{-2}$).

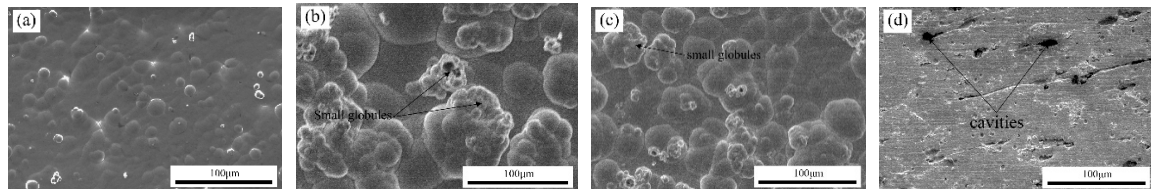


Figure 4. SEM images of the surface morphologies of Ni-11.0W/Cr₂O₃ nanocomposite coatings deposited at different Cr₂O₃ concentrations: (a) $2 \text{ g}\cdot\text{L}^{-1}$, (b) $6 \text{ g}\cdot\text{L}^{-1}$, (c) $10 \text{ g}\cdot\text{L}^{-1}$, and (d) $20 \text{ g}\cdot\text{L}^{-1}$ ($i_d = 1 \text{ A}\cdot\text{dm}^{-2}$).

Figure 5a,b shows cross sections of the Ni-W and Ni-W/Cr₂O₃ coatings obtained using SEM. The figures show that the Ni-W and Ni-W/Cr₂O₃ coatings both exhibited a compact structure with good adherence of the coating matrices to the surface and a uniform thickness was observed for both coatings.

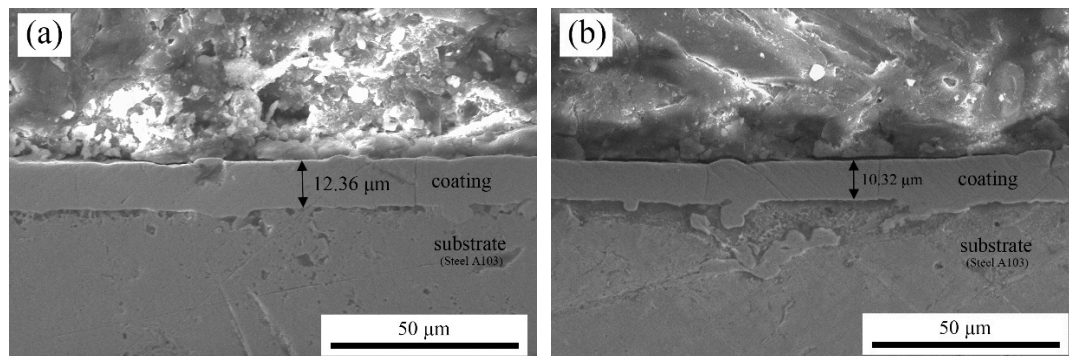


Figure 5. Cross-section images of (a) Ni-W binary alloy coating ($40 \text{ g}\cdot\text{L}^{-1}$ of W and $1 \text{ A}\cdot\text{dm}^{-2}$), and (b) Ni-W/Cr₂O₃ nanocomposite coating ($10 \text{ g}\cdot\text{L}^{-1}$ of Cr₂O₃ and $1 \text{ A}\cdot\text{dm}^{-2}$).

From the current efficiency analysis, it was found that Ni-W coatings with 11.0 wt.% W content had a current efficiency of 42.05% compared to 32.82% for Ni-W/Cr₂O₃ electrodeposited with $10 \text{ g}\cdot\text{L}^{-1}$ Cr₂O₃ nanoparticles. Addition of nanoparticles into the electrolyte caused a reduction in the current efficiency as well as the coating thickness. Also, there was a subsequent reduction of the capturing capacity of nanoparticles. As a result, there was loose adsorption and low Cr₂O₃ nanoparticle content in the deposited coatings evidenced by the low Cr₂O₃ contents reported. It can be suggested that the Cr₂O₃ nanoparticles hindered the diffusion of the metallic ions through the electrolyte bulk to the cathode surface thereby reducing metal electrodeposition rate. The same phenomenon was reported by Yariand Dehghanian [23].

3.2.2. Effects of Cr₂O₃ Nanoparticles on Ni-W/Cr₂O₃ Nanocomposites

Figure 6 shows the variation of deposited Cr₂O₃ and W contents (wt.%) as a function of concentration of Cr₂O₃ nanoparticles with a current density of $1 \text{ A}\cdot\text{dm}^{-2}$ and deposition time of 1 h. It can be seen that the wt.% of Cr₂O₃ content in the coating is dependent on the concentration of Cr₂O₃ in the electrolyte [32].

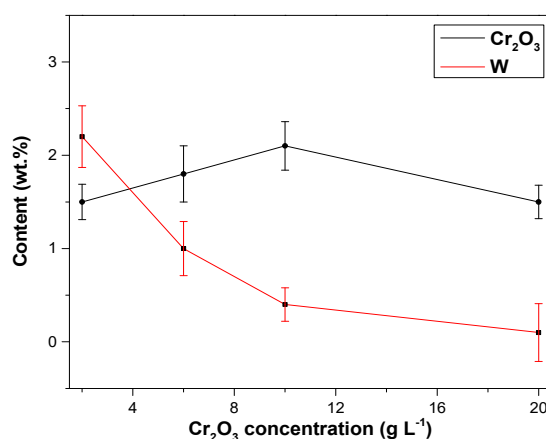


Figure 6. Effect of Cr₂O₃ nano-particle concentration on Cr₂O₃ nano-particle and W content in the Ni-W/Cr₂O₃ nanocomposite coatings. ($i_d = 1 \text{ A}\cdot\text{dm}^{-2}$). For every concentration of Cr₂O₃ nanoparticles in the electrolyte, three sample measurements were made and the standard deviation of the value range is reflected by the error bars.

The nanoparticle content increased significantly with increase in nanoparticle concentration in the electrolyte bath reaching a maximum of 2.1 wt.% at a concentration of 10 g L⁻¹. Celis' model [33] suggests that charging of particles and transfer through the electrolyte bulk occurs in a five-step process. The Cr₂O₃ nanoparticles undergo particle charging by adsorbing positive ions and acquire a positive surface charge. They are then transferred through the electrolyte bulk to the growing Ni-W matrix by electrophoresis force where they become embedded into the coatings [34]. The metal ions in the electrolyte undergo further reduction resulting in stronger adsorption of the Cr₂O₃ nanoparticles onto the metal matrix. This is in line with the physical loose adsorption step of Gugliemi's two-step adsorption model of inert particles [33,35]. Therefore, it can be suggested that a higher concentration of Cr₂O₃ nanoparticles in the plating bath results in additional particle incorporation at locations otherwise inaccessible with lower particle concentration thereby giving a higher deposited content (wt.%) of Cr₂O₃ nanoparticles [36].

Beyond the maximum, it can be seen that the content of deposited nanoparticles declined steadily with further increase in nanoparticle concentration in the electrolyte. It can be suggested that as more and more nanoparticles deposited into the growing Ni-W matrix, there is subsequent decrease in the active cathode surface available for deposition. This can also be attributed to particle agglomeration and settling [36]. Kuo et al. [37] reported that nanoparticles have a strong tendency of agglomerating in galvanic baths owing to high surface activity from constant Brownian motion in the electrolyte. As a result, the electroplating baths usually have high net attraction energy between particles, which enhances particle agglomeration. At high ionic strength or low surface charge, the nanoparticles undergo irreversible agglomeration [37,38]. Homogeneity of nanoparticle distribution in the matrix is crucial to optimizing the coatings properties since clustering of the nanoparticles contributes significantly to non-uniform stress distribution which promotes damage of the material [39,40]. Similarly, individual nanoparticles have been known to have a greater deposition efficiency compared to agglomerated particle groups [37]. Also, agglomeration of nano particles in the matrix drastically degrades the tribological, mechanical, and corrosion properties of the electrodeposited coatings. For many metal matrix composites, the content of nanoparticles in the coatings increases continuously with increase in nanoparticle concentration up to a maximum limiting value beyond which it decreases [36]. This effect is attributed to adsorption of nanoparticles in the coatings in line with a Langmuir adsorption isotherm, which also correlates to Gugliemi's proposed model of particle adsorption. Concurrently, W content in the Ni-W/Cr₂O₃ nanocomposite coatings was seen to reduce with increase in the Cr₂O₃ concentration in the electrolyte from 2 g·L⁻¹ to 30 g·L⁻¹.

3.2.3. Effect of Current Density on Morphologies of Ni–W/Cr₂O₃ Nanocomposites

Figure 7 shows the surface morphologies of the Ni–W/Cr₂O₃ nanocomposite coatings electrodeposited at varying current densities. From the images, it is evident that the applied current density had a tremendous effect on the growth and microstructure of Ni–W/Cr₂O₃ coatings. Particle agglomeration on the surface of the coatings can be attributed to insufficient dispersion of Cr₂O₃ nanoparticles in the plating solution. When current density increased from 1 A·dm^{−2} to 3 A·dm^{−2}, it can be seen that the crystal grains of the composite coatings became more distinct [41]. Increase in current density from 1 to 2 A·dm^{−2} resulted in an increase in the Coulomb force that exists between the cathode surface and the adsorbed metal ions and this increased the content of Cr₂O₃ nanoparticles in the deposited coatings from 2.1 wt.% to 2.6 wt.%, respectively (see EDS Figure 8). Current increase had both a desired and detrimental effect to the deposited Ni–W/Cr₂O₃ coatings. Higher current density allows for higher composite coatings growth rate. This however does not necessarily translate to better coatings, because higher current densities pave the way for creation of internal stresses, which once accumulated, lead to crack formation and propagation [41]. It was observed that dense and compact Ni–W/Cr₂O₃ coatings were obtained at current densities below 1 A·dm^{−2} in line with existing literature [19].

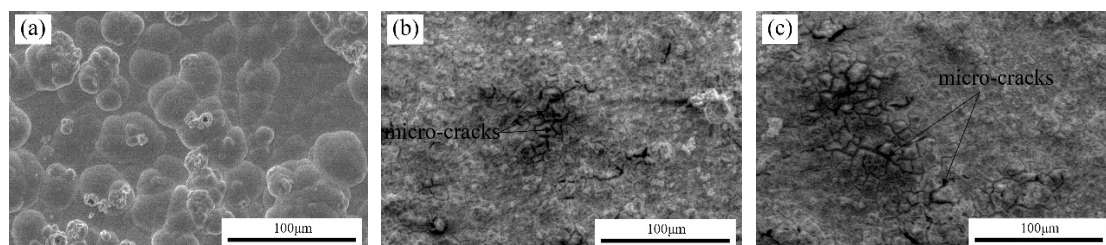


Figure 7. SEM images of the surface morphologies of Ni–W–Cr₂O₃ coatings deposited at different current density (a) 1 A·dm^{−2}, (b) 2 A·dm^{−2}, and (c) 3 A·dm^{−2} (W = 40 g·L^{−1}, C_{Cr₂O₃} = 10 g·L^{−1}).

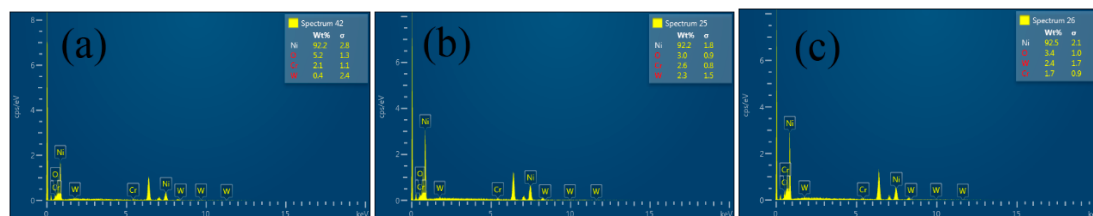


Figure 8. EDS spectra of Ni–W–Cr₂O₃ nanocomposite coatings electrodeposited with 40 g·L^{−1} W and 10 g·L^{−1} Cr₂O₃ concentrations at (a) 1, (b) 2, and (c) 3 A·dm^{−2}.

3.2.4. Effect of Current Density on Properties of Ni–W/Cr₂O₃ Nanocomposites

The influence of varying current density on the nanocomposite coatings composition was analyzed by considering the contents of Cr₂O₃ in the deposited Ni–W/Cr₂O₃ coatings. Ni–W/Cr₂O₃ nanocomposites electrodeposited at 1 A·dm^{−2} with 40 g·L^{−1} W and 10 g·L^{−1} Cr₂O₃ exhibited the best corrosion resistance and microhardness properties. As such, these samples were selected to evaluate the effect of varying current density.

Figure 8 shows the EDS spectra of the Ni–W/Cr₂O₃ nanocomposites electrodeposited at varying current densities with a deposition time of 60 min and a concentration of 10 g·L^{−1} Cr₂O₃. Below a current density of 2 A·dm^{−2}, the Cr₂O₃ nanoparticles influx toward the cathode increased, and this marked the highest value for the Cr₂O₃ content in the coatings. Beyond 2 A·dm^{−2}, the Cr₂O₃ content decreased as a result of increased deposition of Ni metal matrix at a rate much higher than the embedding rate of Cr₂O₃ nanoparticles into the coatings. There was a relatively low concentration of W in all EDS pictographs owing to the absence of ammonium chloride in the electrolyte solutions. It is evident that the predominant element in the coatings was Ni, which sees a deviation from

results reported by Zhang et al. [21]. This can be related to the composition of electrolyte bath used. Yamasaki et al. [17] reported that NH_4Cl concentrations in the bath strongly influenced W content in the deposited coatings, where an increase in NH_4Cl causes a sharp increase in W content.

Figure 9 shows the percentage of codeposited W and Cr_2O_3 as a function of varying current density from a plating bath containing $10 \text{ g L}^{-1} \text{ Cr}_2\text{O}_3$. It can be seen that the Cr_2O_3 content increased steadily with increase in current density until it reached a maximum of 2.6 wt.% at $2 \text{ A}\cdot\text{dm}^{-2}$. This increase can be attributed to increase in nanoparticle adsorption rate into the coatings. Further increase in current density resulted in a decrease in weight percentage of codeposited Cr_2O_3 . Lower current densities exhibited higher Cr_2O_3 nanoparticles content and this can be attributed to an increase in the adsorbed nanoparticles arriving at the cathode surface. From past literature, it is assumed that mass transportation rate of nanoparticles and cations to the cathode surface determines the content of nanoparticles deposited into the coatings. Increase in current density to a certain optimal value results in a subsequent rise in transfer of charged nanoparticles through the electrolyte bulk, which in turn increases the adsorption rate of nanoparticles on the growing Ni–W matrix. However, this increase in nanoparticle content with increase in current density is faced by a corresponding challenge. Increase in current density beyond $2 \text{ A}\cdot\text{dm}^{-2}$ has a detrimental effect on nanoparticle deposition because the metal ions in the electrolytic solution are transferred at a much faster rate (electrolytic) to the cathode than the nanoparticles (mechanical agitation) [42]. It can also be suggested that at higher current density ($3 \text{ A}\cdot\text{dm}^{-2}$), there is increased polarization tendency, which increases hydrogen evolution at the electrode, which may lead to lowering of content of Cr_2O_3 nanoparticles in the electrodeposited coatings [41].

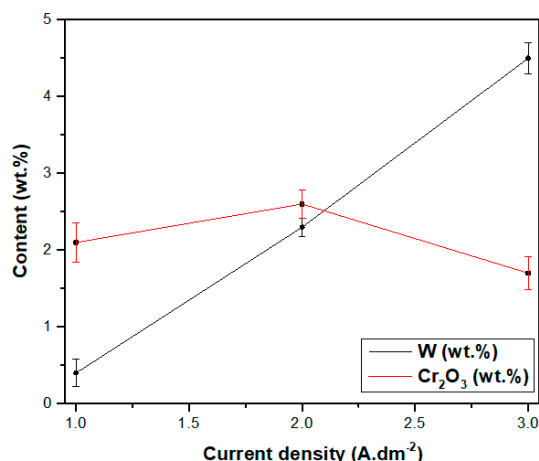


Figure 9. Effect of current density on the composition of Ni–W/ Cr_2O_3 nanocomposite coatings (Cr_2O_3 $10 \text{ g}\cdot\text{L}^{-1}$, plating time 60 min). The error bars represent a standard error resulting from data taken from four similar samples for each current density.

From Figure 9, it is evident that content of W increased continuously with increase in current density. This is as a result of static potential reduction of the Ni–W alloy as compared to the individual metals [43]. This is concurrent with conclusions drawn by Sriraman et al. [9]. The highest W content of 2.4 wt.% was achieved at the highest applied current density of $3 \text{ A}\cdot\text{dm}^{-2}$. The highest content of Cr_2O_3 nanoparticles (2.6 wt.%) was achieved at $2 \text{ A}\cdot\text{dm}^{-2}$.

3.2.5. XRD Spectrum of Coatings

Figure 10a,b shows the XRD patterns of the electrodeposited Ni–W and Ni–W/ Cr_2O_3 coatings with varying quantities of W and Cr_2O_3 nanoparticles in the electrolyte, respectively. Ni–W/ Cr_2O_3 alloy coatings patterns exhibited five distinct peaks at $2\theta = 44.5^\circ, 44.7^\circ, 51.8^\circ, 76.4^\circ,$ and 82.4° , and these correlated to (111), (110), (200), (220), and (211) crystallographic FCC planes of Ni, respectively [18]. It is evident that the Ni–W/ Cr_2O_3 nanocomposite coatings consisted of crystalline face centred cubic (FCC)

structure comprising of both Ni–W alloy and Cr_2O_3 nanoparticles [44]. Increase in W concentration resulted in a subsequent fall in the Ni (110), (111), and (200) lattices and a rise in the (211) lattice. The lowering of the peak intensity and broadening of the peaks for the Ni–W matrix alloy suggests there was incorporation of W atoms, which have a 10% larger atomic radius as compared to Ni atoms into the FCC Ni lattice (Ni = 1.224 Å, W = 1.371 Å [18,45]). Ni and W combined to form a solid solution, where the W atoms displaced some Ni atoms into the FCC Ni lattice. With increase in W content in the coatings, the Ni content decreased and phase structure was distorted owing to a change in crystallite size. The reduction in crystallite size with increase in the alloying element (W) in the coatings results in the broadening of the lattice peaks [9]. The incorporation of W atoms into the Ni lattice causes the FCC lattice to expand, thereby shifting the Bragg angle peaks to lower scattering angles [18]. It can be seen from Figure 10b that an increase in Cr_2O_3 nanoparticle concentration in the electrolyte led to a significant fall in the peak intensity for the Nickel (111) and (200) planes with no shift in peak positions, and this is attributed to formation of Ni–W solid solution and successful deposition of the Cr_2O_3 nanoparticles into the Ni–W/ Cr_2O_3 nanocomposite coating. Considering the inclination of the Ni–W/ Cr_2O_3 coatings towards an amorphous structure, it can also be suggested that the deposited Cr_2O_3 nanoparticles provided nucleation sites resulting in formation of nano crystallites [41]. These changes in the structure resulted in Ni–W/ Cr_2O_3 nanocomposite coatings with improved strength. There were no distinct peaks for chromium element in the XRD patterns owing to the small sizes of Cr_2O_3 nanoparticles used (20 nm) and the relatively low concentrations of Cr_2O_3 nanoparticles. The successful incorporation of the Cr_2O_3 nanoparticles into the coatings is, however, evident in EDS pictographs (Figure 8a–c).

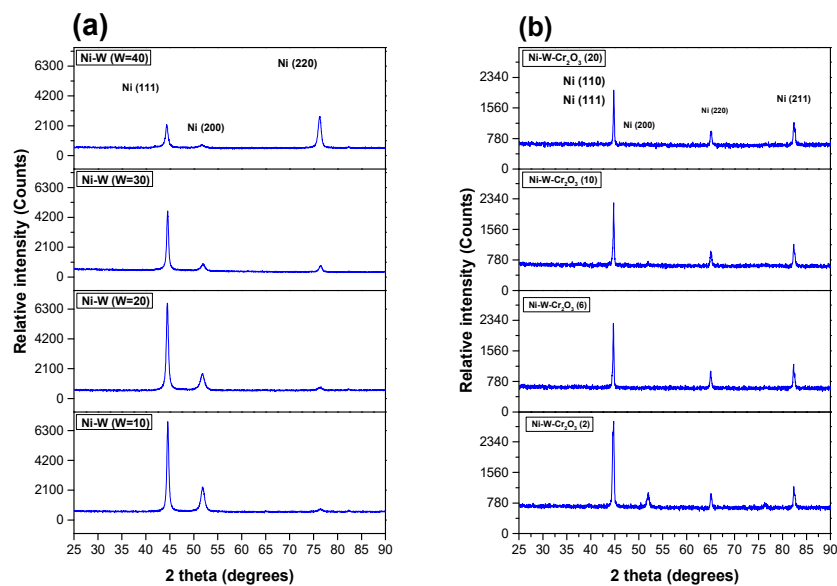


Figure 10. (a). XRD diffraction patterns for Ni–W binary alloys electrodeposited with varying concentrations of W (10, 20, 30, and 40 $\text{g}\cdot\text{L}^{-1}$); (b). XRD diffraction patterns for Ni–W/ Cr_2O_3 electrodeposited with varying concentrations of Cr_2O_3 (2, 6, 10, and 20 $\text{g}\cdot\text{L}^{-1}$).

Figure 11 shows the XRD patterns of Ni–W/ Cr_2O_3 nanocomposite coatings electrodeposited at different current densities of 1, 2, and 3 $\text{A}\cdot\text{dm}^{-2}$ (0.4 wt.% W and 2.1 wt.% Cr_2O_3). It can be seen that the main Bragg peaks were located at $2\theta = 44.5^\circ$, 44.7° , 51.8° , 76.4° , and 82.3° , which corresponded to the diffraction of the (110), (111), (200), (220), and (211) lattice planes of fcc, respectively. There was no substantial change in peak positions for the Ni–W/ Cr_2O_3 nanocomposites, but there is clear indication that varying current density influenced the peak intensities. Increase in current density from 1 $\text{A}\cdot\text{dm}^{-2}$ to 3 $\text{A}\cdot\text{dm}^{-2}$ caused a rise in peak intensity for the (110), (111), and (200) indexes while the intensity of (211) was decreased.

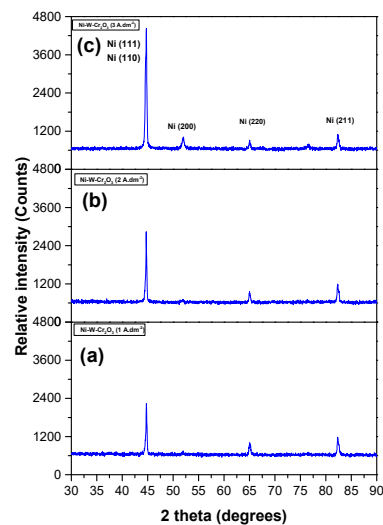


Figure 11. XRD diffraction patterns for Ni–W–Cr₂O₃ with 2.1 wt.% Cr₂O₃ content electrodeposited at (a) 1, (b) 2, and (c) 3 A·dm^{−2}.

3.2.6. Microhardness and Wear Behavior

Figure 12 shows the microhardness of the Ni-11.0W/Cr₂O₃ nanocomposite coatings as a function of the content of Cr₂O₃ in the deposited coatings. It can be seen that the microhardness increased with increase in the content of Cr₂O₃ in the coatings, such that all the Ni-11.0W/Cr₂O₃ nanocomposite coatings exhibited better microhardness compared to the purely Ni–W alloy coatings. Similar observations were made by Zhang et al. [21]. Ni–W binary alloy coatings fabricated under similar conditions exhibited microhardness of 498 HV. This increase in microhardness can be attributed to grain refining and dispersive strengthening effect (uniform distribution) of the Cr₂O₃ nanoparticles in the Ni–W matrix, which increases the load bearing capacity of the coatings, hinders plastic deformation during loading, and restrains growth of Ni–W grains [46]. It is clear that the microhardness of the Ni-11.0W/Cr₂O₃ nanocomposite coatings increased with increase in Cr₂O₃ concentration until a maximum value, beyond which the microhardness decreases [47]. From past literature, it can be suggested that the main strengthening mechanism is Cr₂O₃ nanoparticle dispersion in the Ni-11.0W/Cr₂O₃ coatings, where smaller sizes of nanoparticles and shorter distances between the particles improve the overall properties of the coatings [48]. The embedded Cr₂O₃ nanoparticles act as fibers in the Ni–W matrix to prevent creation and propagation of micro-cracks. Dispersive strengthening as a result of grain refining is observed with increase in the content of deposit Cr₂O₃ nanoparticles in the coatings. The maximum microhardness of 602 HV is achieved where coatings have 2.1 wt.% content of Cr₂O₃. The effect of high microhardness at significantly lower contents of Cr₂O₃ (2.1 wt.%) can be attributed to the stronger bonding strength between Ni–W matrix and the dispersed Cr₂O₃ nanoparticles of lower content compared to that of higher Cr₂O₃ content, which tends to agglomerate [47].

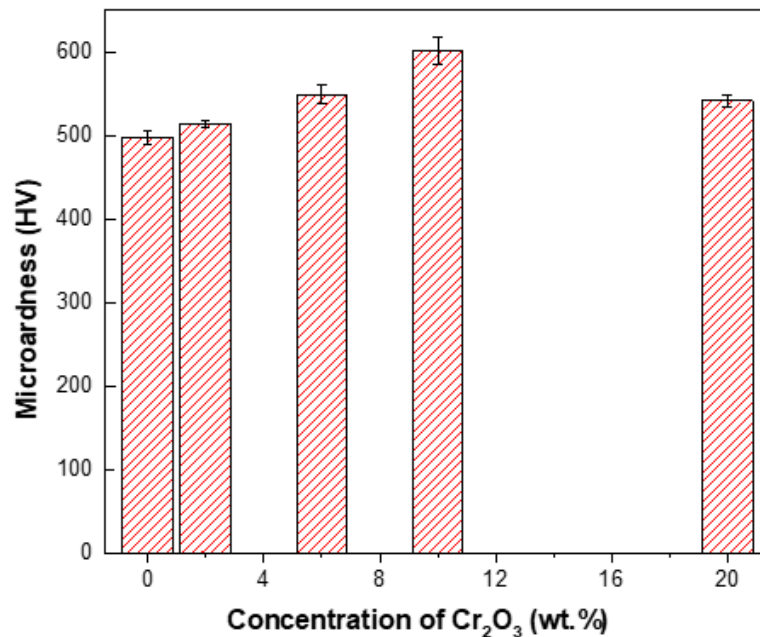


Figure 12. Microhardness of electrodeposited Ni–W/Cr₂O₃ with varying concentrations of Cr₂O₃ in the coatings. The standard deviation from the performed measurements range of values obtained from the 10 separate indentation measurements of each sample is represented by the error bars.

The highest microhardness readings for the Ni–W and Ni–W/Cr₂O₃ coatings electrodeposited at $1 \text{ A}\cdot\text{dm}^{-2}$ were 498 HV and 602 HV, respectively. As such, samples electrodeposited with these parameters were selected for wear analysis. Figure 13 displays the coefficient of friction (COF) patterns of the Ni–W binary alloy coating and the Ni–W/Cr₂O₃ nanocomposite coatings. It is evident that the friction coefficient of Ni–W was about 0.6 ± 0.1 with a relatively uniform curve. Incorporation of Cr₂O₃ nanoparticles into the Ni–W matrix resulted in a shift in this friction curve. It can be seen that the COF decreased to 0.48 ± 0.1 for the Ni–W/Cr₂O₃ coatings. This can be associated with successful adsorption of Cr₂O₃ nanocomposites into the structure. It can be suggested that the Cr₂O₃ nanoparticles became dislodged from the coating, which caused a lowering of the wear rate as a result of wear mode transformation from sliding mode to rolling mode [49]. As such, it can be concluded that the wear rate of Ni–W/Cr₂O₃ is less compared to Ni–W binary alloy coatings.

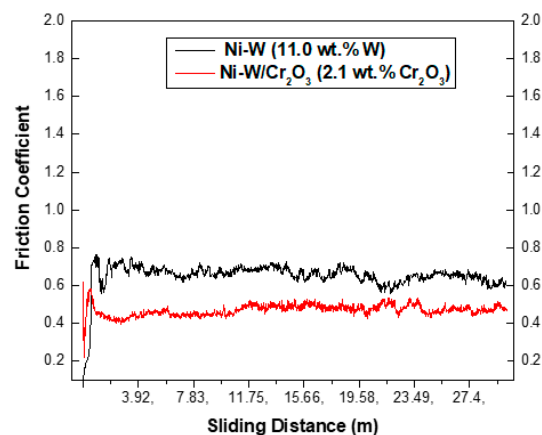


Figure 13. Typical curve of the friction coefficient of Ni–W binary alloy coatings (11.0 wt.% W), and Ni–W/Cr₂O₃ (2.1 wt.% Cr₂O₃) nanocomposite coatings.

Figure 14a,b shows the wear grooves for the Ni–W and Ni–W/Cr₂O₃ coatings, respectively. From Figure 14a it can be seen that the groove for the Ni–W binary coating with 11.0 wt.% W content was

729 μm . The high quantity of plough lines and adhesive tearing along the direction of sliding suggests that there was a combination of adhesive and abrasive wear mechanisms on the Ni–W alloy [50]. After successful incorporation of Cr_2O_3 nanoparticles into the Ni–W binary alloy matrix, the plough lines became shallower and the groove width for the Ni–W/ Cr_2O_3 nanocomposite coating with 2.1 wt.% Cr_2O_3 content reduced to 499 μm as shown in Figure 14b. The abrasive grooves in Ni–W/ Cr_2O_3 were less pronounced compared to those of binary Ni–W coatings and this shows an increased resistance to wear. The Cr_2O_3 nanoparticles provide both particle strengthening and dispersion strengthening which improves the wear resistance of Ni–W/ Cr_2O_3 [51]. Also, the Cr_2O_3 nanoparticles may act as solid lubricants between the surfaces in contact thereby mitigating wear of the deposits. Similar results suggesting that adsorption of nanoparticles improves wear resistance were reported by Yao [52].

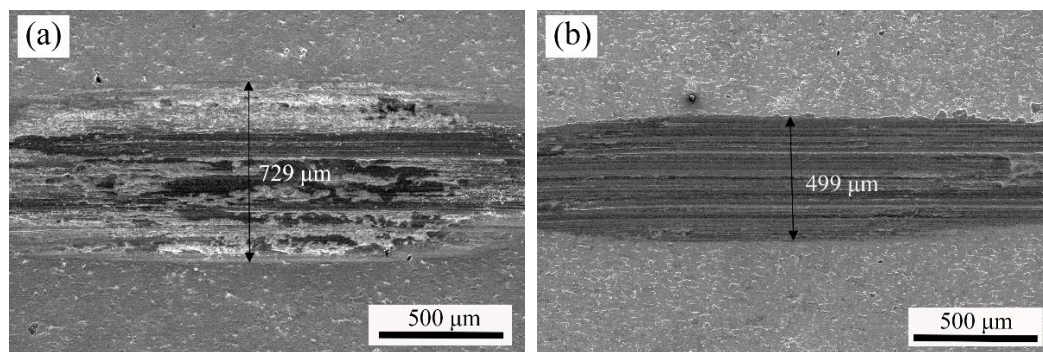


Figure 14. SEM micrographs of worn surfaces of (a) Ni–W coatings with 11.0 wt.% W content and (b) Ni–W/ Cr_2O_3 composite coatings with 2.1 wt.% Cr_2O_3 content.

3.2.7. Corrosion Resistance

Potentiodynamic polarization measurements for the Ni-11.0W/ Cr_2O_3 nanocomposite coatings with varying contents of Cr_2O_3 electrodeposited at $1 \text{ A}\cdot\text{dm}^{-2}$ were evaluated. The samples were first immersed into the 3.5 wt.% NaCl corrosive medium until E_{ocp} was attained. The effect of increase in Cr_2O_3 concentration in the electrolyte on corrosion resistance of Ni–W/ Cr_2O_3 coatings was analyzed.

Figure 15 shows the potentiodynamic polarization curves of Ni-11.0W/ Cr_2O_3 coatings electrodeposited with varying concentrations of Cr_2O_3 as a function of time.

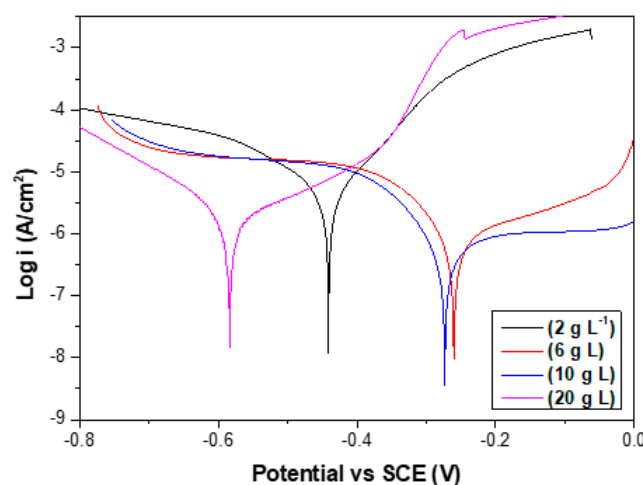


Figure 15. Potentiodynamic polarization curves of the Ni–W/ Cr_2O_3 coatings as a function of the Cr_2O_3 nanoparticle concentration in the electrolyte (current density = $1 \text{ A}\cdot\text{dm}^{-2}$).

Tafel extrapolation and linear polarization resistance methods were used to obtain the corrosion potential E_{corr} , corrosion current density i_{corr} , and polarization resistance R_p . Table 6 summarizes the potentiodynamic polarization data of the Ni-11.0W/Cr₂O₃ coatings for comparison purposes.

Table 6. Electrochemical data from potentiodynamic polarization curves of the Ni-W-Cr₂O₃ as a function of Cr₂O₃ nanoparticle concentration in the electrolyte. ($i_d = 1 \text{ A}\cdot\text{dm}^{-2}$).

Coatings	Concentration (g·L ⁻¹)	β_a (mV)	β_c (mV)	E_{corr} (Volts)	i_{corr} ($\mu\text{A}\cdot\text{cm}^{-2}$)	Corrosion Rate (mm/a)	R_p ($\text{k}\Omega\cdot\text{cm}^{-2}$)
Ni-11W	0	395.48	545.57	-0.42606	22.461	0.27186	4.432
Ni-11W-Cr ₂ O ₃	2	99.98	173.41	-0.44098	5.585	0.06760	4.929
Ni-11W-Cr ₂ O ₃	6	4734.70	170.88	-0.26004	2.615	0.03165	27.382
Ni-11W-Cr ₂ O ₃	10	171.66	82.08	-0.27321	0.553	0.00670	43.540
Ni-11W-Cr ₂ O ₃	20	1084.40	240.69	-0.58341	5.832	0.07058	14.665

From Table 6, it is clear that polarization resistance R_p of Ni-11.0W binary alloy coatings was less than that of Ni-11.0W/Cr₂O₃ composite coatings. This increase in corrosion resistance with increase in Cr₂O₃ content can be attributed to reduction of the coating's exposed effective area to the corrosive NaCl medium. Also, to be considered is the small size of the nanoparticles selected for deposition. Research shows that coatings embedded with nano-sized particles exhibit better corrosion resistance compared to those embedded with macro-sized particles [34]. The nano-sized particles can easily penetrate and fill the submicron defects in the coatings, while microscale particles are unable to. As such, small particle sizes of Cr₂O₃ nanoparticles coupled with their distribution in the coatings could be contributing factors that could have promoted the high corrosion resistance of Ni-11.0W/Cr₂O₃ composite coatings. The ceramic Cr₂O₃ nanoparticles also act as physical barriers, which hinder initiation and propagation of corrosion defects created by the corrosive NaCl medium [20]. Another factor that could explain the higher corrosion resistance of composite coatings over binary alloy coatings is alteration of corrosion mechanism at the matrix-reinforcement interface from localized to uniform. Chen et al. [53] researched corrosion behavior of carbon nanotubes in Ni matrix composite coatings. It was found that dispersion of the reinforcement particles in the Ni matrix created micro-galvanic cells where Ni metal acted as the anode and reinforcing particles acted as cathodes. Increase in Cr₂O₃ concentration from 2 g·L⁻¹ to 10 g·L⁻¹ results in an increase in polarization resistance (R_p) from 4.929 $\text{k}\Omega\cdot\text{cm}^{-2}$ to 43.540 $\text{k}\Omega\cdot\text{cm}^{-2}$, and this marks the highest value of polarization resistance achieved for the Ni-11.0W/Cr₂O₃ composite coatings. Beyond a certain concentration of Cr₂O₃ in the plating bath, the corrosion resistance decreases. This decline can be attributed to increase in density of the grain boundaries. Grain boundaries form a weak point in coatings owing to their higher levels of energy compared to the inner sections of the materials, and corrosive attacks tend to be more concentrated at these locations.

Figure 16 shows the effect of current density on the potentiodynamic polarization curves of the Ni-W/Cr₂O₃ nanocomposite coatings. Data extracted from the curves are presented in Table 7 for comparison purposes.

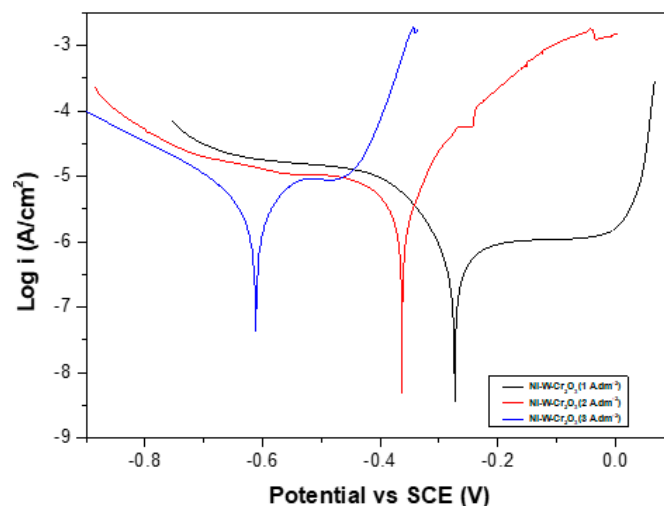


Figure 16. Potentiodynamic polarization curves of the Ni-W/Cr₂O₃ coatings as a function of the plating current density (W = 0.4 wt.%, Cr₂O₃ = 2.1 wt.%).

Table 7. Electrochemical data from potentiodynamic polarization curves of the Ni-W/Cr₂O₃ as a function of deposition current density (W = 0.4 wt.%, Cr₂O₃ = 2.1 wt.%).

Coatings	Current Density (A·dm ⁻²)	β_a (mV)	β_c (mV)	E_{corr} (Volts)	i_{corr} ($\mu\text{A}\cdot\text{cm}^{-2}$)	Corrosion Rate (mm/a)	R_p ($\text{k}\Omega\cdot\text{cm}^{-2}$)
Ni-yyW-xxCr ₂ O ₃	1	171.66	82.089	-0.27321	0.5538	0.006702	43.54
Ni-yyW-xxCr ₂ O ₃	2	100.78	514.98	-0.36289	6.1465	0.074394	5.9543
Ni-yyW-xxCr ₂ O ₃	3	3444.2	450.06	-0.61182	18.656	0.2258	9.2645

From the data, it can be seen that the corrosion current density (i_{corr}) increased with increase in current density from $0.5538 \mu\text{A}\cdot\text{cm}^{-2}$ at $1 \text{ A}\cdot\text{dm}^{-2}$ to $18.656 \mu\text{A}\cdot\text{cm}^{-2}$ at $3 \text{ A}\cdot\text{dm}^{-2}$. The lowest corrosion current density value of $0.5538 \mu\text{A}\cdot\text{cm}^{-2}$ was achieved at $1 \text{ A}\cdot\text{dm}^{-2}$. As such, it can be concluded that the Ni-W/Cr₂O₃ nanocomposite coatings containing 0.4 wt.% W and 2.1 wt.% Cr₂O₃ nanoparticles electrodeposited at $1 \text{ A}\cdot\text{dm}^{-2}$ exhibited the best polarization resistance.

4. Conclusions

Several conclusions have been drawn from the results obtained in the experiment:

- (i) Corrosion resistance of Ni-W binary alloys increased significantly with increase in W content in the coating for the range of W concentration used in this experiment ($10 \text{ g}\cdot\text{L}^{-1}$ to $40 \text{ g}\cdot\text{L}^{-1}$).
- (ii) The nanoparticle content in the Ni-W/Cr₂O₃ nanocomposite coatings increased with increase in Cr₂O₃ nanoparticle concentration in the electrolyte.
- (iii) SEM images showed that the surface morphology of Ni-W/Cr₂O₃ nanocomposite coatings was nodular at $2 \text{ g}\cdot\text{L}^{-1}$, had elliptical clusters comprising of small globules at $6 \text{ g}\cdot\text{L}^{-1}$ and $10 \text{ g}\cdot\text{L}^{-1}$, and a more amorphous tendency characterized by cavities at $20 \text{ g}\cdot\text{L}^{-1}$. Ni-W/Cr₂O₃ composites deposited at $2 \text{ A}\cdot\text{dm}^{-2}$ and $3 \text{ A}\cdot\text{dm}^{-2}$ are characterized by a dense net of micro-cracks.
- (iv) Ni-W/Cr₂O₃ nanocomposite coatings electrodeposited with $40 \text{ g}\cdot\text{L}^{-1}$ W and $10 \text{ g}\cdot\text{L}^{-1}$ Cr₂O₃ in electrolyte exhibited the best microhardness. It should be noted that these coatings represent only those electrodeposited at $1 \text{ A}\cdot\text{dm}^{-2}$.
- (v) Ni-W/Cr₂O₃ nanocomposites exhibits superior wear resistance properties compared to Ni-W binary alloy coatings with coatings deposited with $10 \text{ g}\cdot\text{L}^{-1}$ Cr₂O₃ concentration exhibiting the best wear resistance.
- (vi) Ni-W/Cr₂O₃ nanocomposite coatings electrodeposited with $40 \text{ g}\cdot\text{L}^{-1}$ W and $10 \text{ g}\cdot\text{L}^{-1}$ Cr₂O₃ in electrolyte at $1 \text{ A}\cdot\text{dm}^{-2}$ exhibited the best corrosion resistance.

Author Contributions: Conceptualization, S.M.N. and M.K.; methodology, S.M.N., and Y.L.; validation, S.M.N. and M.K.; formal analysis, S.M.N. and Y.Z.; investigation, S.M.N., Y.Z., and N.J.N.; resources, M.K.; writing—original draft preparation, S.M.N. and N.J.N.; writing—review and editing, S.M.N. and M.K.; visualization, S.M.N., Y.Z., and Y.L.; supervision, M.K.; project administration, M.K. and J.Z.; funding acquisition, M.K.

Funding: The research was funded by the Technology development programmer for the Northern Jiangsu area, (Grant No. BN2014019).

Acknowledgments: EDS spectra of the Ni-W and Ni-W/Cr₂O₃ nanocomposite coatings was analysed by Research Institute of Nanjing Chemical Industry Group, Sinopec.

Conflicts of Interest: The authors declare no conflict of interest.

References

1. Hansson, C.J.M. The impact of corrosion on society. *Metall. Mater. Trans. A* **2011**, *42*, 2952–2962. [[CrossRef](#)]
2. Ibrahim, I.A.; Mohamed, F.A.; Lavernia, E.J. Particulate reinforced metal matrix composites—A review. *J. Mater.* **1991**, *26*, 1137–1156. [[CrossRef](#)]
3. Bhushan, B.; Gupta, B.K. *Handbook of Tribology: Materials, Coatings, and Surface Treatments*; Stanford Libraries: Stanford, CA, USA, 1991.
4. Aghajanian, M.K.; Rocazella, M.A.; Burke, J.T.; Keck, S.D. The fabrication of metal matrix composites by a pressureless infiltration technique. *J. Mater.* **1991**, *26*, 447–454. [[CrossRef](#)]
5. Robertson, A.; Erb, U.; Palumbo, G. Practical applications for electrodeposited nanocrystalline materials. *Nanostruct. Mater.* **1999**, *12*, 1035–1040. [[CrossRef](#)]
6. Landolt, D. Electrochemical and materials science aspects of alloy deposition. *Electrochim. Acta* **1994**, *39*, 1075–1090. [[CrossRef](#)]
7. Gurrappa, I.; Binder, L. Materials, Electrodeposition of nanostructured coatings and their characterization—A review. *Sci. Technol. Adv. Mater.* **2008**, *9*, 043001. [[CrossRef](#)]
8. Low, C.T.; Wills, R.G.; Walsh, F.C. Electrodeposition of composite coatings containing nanoparticles in a metal deposit. *Surf. Coat. Technol.* **2006**, *201*, 371–383. [[CrossRef](#)]
9. Sriraman, K.R.; Raman, S.G.; Seshadri, S.K. Corrosion behaviour of electrodeposited nanocrystalline Ni–W and Ni–Fe–W alloys. *Mater. Sci. Eng. A* **2007**, *460*, 39–45. [[CrossRef](#)]
10. Genç, A.; Öveçoğlu, M.L.; Baydoğan, M.; Turan, S. Fabrication and characterization of Ni–W solid solution alloys via mechanical alloying and pressureless sintering. *Mater. Des.* **2012**, *42*, 495–504. [[CrossRef](#)]
11. Galikova, Z.; Chovancova, M.; Danielik, V. Danielik, Properties of Ni–W alloy coatings on steel substrate. *Chem. Pap.* **2006**, *60*, 353–359. [[CrossRef](#)]
12. Popov, K.; Grgur, B.; Djokić, S.S. *Fundamental Aspects of Electrometallurgy*; Springer Science & Business Media: Berlin, Germany, 2007.
13. Alimadadi, H.; Ahmadi, M.; Aliofkhaezrai, M.; Younesi, S.R. Corrosion properties of electrodeposited nanocrystalline and amorphous patterned Ni–W alloy. *Mater. Des.* **2009**, *30*, 1356–1361. [[CrossRef](#)]
14. De Lima-Neto, P.; Correia, A.N.; Santana, R.A.; Colares, R.P.; Barros, E.B.; Casciano, P.N.; Vaz, G.L. Morphological, structural, microhardness and electrochemical characterisations of electrodeposited Cr and Ni–W coatings. *Electrochim. Acta* **2010**, *55*, 2078–2086. [[CrossRef](#)]
15. Landolt, D. Finishing, Fundamental aspects of alloy plating. *Plat. Surf. Finish.* **2001**, *88*, 70.
16. Donten, M.; Cesiulis, H.; Stojek, Z. Electrodeposition and properties of Ni⁸⁵W, Fe⁸⁵W and Fe⁸⁵Ni¹⁵W amorphous alloys. A comparative study. *Electrochim. Acta* **2000**, *45*, 3389–3396. [[CrossRef](#)]
17. Yamasaki, T.; Schloßmacher, P.; Ehrlich, K.; Ogino, Y. Formation of amorphous electrodeposited Ni–W alloys and their nanocrystallization. *Nanostruct. Mater.* **1998**, *10*, 375–388. [[CrossRef](#)]
18. Wasekar, N.P.; Latha, S.M.; Ramakrishna, M.; Rao, D.S.; Sundararajan, G. Pulsed electrodeposition and mechanical properties of Ni–W/SiC nano-composite coatings. *Mater. Des.* **2016**, *112*, 140–150. [[CrossRef](#)]
19. Beltowska-Lehman, E.; Indyka, P.; Bigos, A.; Szczerba, M.J.; Kot, M. Ni–W/ZrO₂ nanocomposites obtained by ultrasonic DC electrodeposition. *Mater. Des.* **2015**, *80*, 1–11. [[CrossRef](#)]
20. Rasooli, A.; Safavi, M.S.; Hokmabad, M.K. Cr₂O₃ nanoparticles: A promising candidate to improve the mechanical properties and corrosion resistance of Ni–Co alloy coatings. *Ceram. Int.* **2018**, *44*, 6466–6473. [[CrossRef](#)]

21. Zhang, Y.; Leng, X.; Wang, X.; Ou, P.; Zhang, W.; Zhou, Q. Electrodeposition and Characterization of Ni–W–Cr 2 O 3 Nanocomposite Coating. *Metallogr. Microstruct. Anal.* **2017**, *6*, 519–526. [[CrossRef](#)]
22. Weil, R.; Cook, H.C. Electron-Microscopic Observations of the Structure of Electroplated Nickel. *J. Electrochem. Soc.* **1962**, *109*, 295–301. [[CrossRef](#)]
23. Yari, S.; Dehghanian, C. Deposition and characterization of nanocrystalline and amorphous Ni–W coatings with embedded alumina nanoparticles. *Ceram. Int.* **2013**, *39*, 7759–7766. [[CrossRef](#)]
24. Stern, M.; Geary, A.L. Electrochemical polarization I. A theoretical analysis of the shape of polarization curves. *J. Electrochem. Soc.* **1957**, *104*, 56–63. [[CrossRef](#)]
25. Brenner, A. Electrodeposition of alloys. *J. Electrochem. Soc.* **1964**, *111*, 34C–35C. [[CrossRef](#)]
26. Gileadi, E.; Eliaz, N. The mechanism of induced codeposition of Ni–W alloys. *ECS Trans.* **2007**, *2*, 337–349.
27. Younes, O.; Gileadi, E. Letters, Electroplating of high tungsten content Ni/W alloys. *Electrochem. Solid-State Lett.* **2000**, *3*, 543–545. [[CrossRef](#)]
28. Miracle, D.B.; Donaldson, S.L.; Henry, S.D.; Moosbrugger, C.; Anton, G.J.; Sanders, B.R.; Hrivnak, N.; Terman, C.; Kinson, J.; Muldoon, K.; et al. *ASM Handbook*; ASM International Materials Park: Geauga, OH, USA, 2003.
29. Tury, B.; Lakatos-Varsányi, M.; Roy, S. Ni–Co alloys plated by pulse currents. *Surf. Coat. Technol.* **2006**, *200*, 6713–6717. [[CrossRef](#)]
30. Allahyarzadeh, M.H.; Aliofkhaezai, M.; Rouhaghdam, A.S.; Torabinejad, V. Electrodeposition of Ni–W–Al₂O₃ nanocomposite coating with functionally graded microstructure. *J. Alloys Compd.* **2016**, *666*, 217–226. [[CrossRef](#)]
31. Eliaz, N.; Sridhar, T.M.; Gileadi, E. Gileadi, Synthesis and characterization of nickel tungsten alloys by electrodeposition. *Electrochim. Acta* **2005**, *50*, 2893–2904. [[CrossRef](#)]
32. Yao, Y.; Yao, S.; Zhang, L.; Wang, H. Electrodeposition and mechanical and corrosion resistance properties of Ni–W/SiC nanocomposite coatings. *Mater. Lett.* **2007**, *61*, 67–70. [[CrossRef](#)]
33. Celis, J.P.; Roos, J.R. Kinetics of the deposition of alumina particles from copper sulfate plating baths. *J. Electrochem. Soc.* **1977**, *124*, 1508–1511. [[CrossRef](#)]
34. Bakhit, B.; Akbari, A. Technology, Effect of particle size and co-deposition technique on hardness and corrosion properties of Ni–Co/SiC composite coatings. *Surf. Coat. Technol.* **2012**, *206*, 4964–4975. [[CrossRef](#)]
35. Gu-ielmi, N. Kinetics of the deposition of inert particles from electrolytic baths. *J. Electrochem. Soc.* **1972**, *119*, 1009–1012. [[CrossRef](#)]
36. Hovestad, A.; Janssen, L.J. Electroplating of metal matrix composites by codeposition of suspended particles, in Modern aspects of electrochemistry. In *Modern Aspects of Electrochemistry*; Springer: Berlin, Germany, 2005; pp. 475–532.
37. Kuo, S.L.; Chen, Y.C.; Ger, M.D.; Hwu, W.H. Nano-particles dispersion effect on Ni/Al₂O₃ composite coatings. *Mater. Chem. Phys.* **2004**, *86*, 5–10. [[CrossRef](#)]
38. Gomes, A.; Pereira, I.; Fernandez, B.; Pereiro, R. Electrodeposition of metal matrix nanocomposites: Improvement of the chemical characterization techniques, in Advances in nanocomposites-synthesis, characterization and industrial applications. In *Advances in Nanocomposites-Synthesis, Characterization and Industrial Applications*; IntechOpen: London, UK, 2011.
39. Wang, Z.; Chen, T.K.; Lloyd, D.J. Stress distribution in particulate-reinforced metal-matrix composites subjected to external load. *Metall. Trans. A* **1993**, *24*, 197–207. [[CrossRef](#)]
40. Benea, L. Electrodeposition and tribocorrosion behaviour of ZrO₂–Ni composite coatings. *J. Appl. Electrochem.* **2009**, *39*, 1671. [[CrossRef](#)]
41. Li, B.; Zhang, W.; Zhang, W.; Huan, Y. Preparation of Ni–W/SiC nanocomposite coatings by electrochemical deposition. *J. Alloys Compd.* **2017**, *702*, 38–50. [[CrossRef](#)]
42. Napłoszek-Bilnik, I.; Budniok, A.; Łosiewicz, B.; Pająk, L.; Łagiewka, E. Electrodeposition of composite Ni-based coatings with the addition of Ti or/and Al particles. *Thin Solid Film.* **2005**, *474*, 146–153. [[CrossRef](#)]
43. Ma, M.; Donepudi, V.S.; Sandi, G.; Sun, Y.K.; Prakash, J. Electrodeposition of nano-structured nickel–21% tungsten alloy and evaluation of oxygen reduction reaction in a 1% sodium hydroxide solution. *Electrochim. Acta* **2004**, *49*, 4411–4416. [[CrossRef](#)]
44. Wang, Y.; Zhou, Q.; Li, K.; Zhong, Q.; Bui, Q.B. Preparation of Ni–W–SiO₂ nanocomposite coating and evaluation of its hardness and corrosion resistance. *Ceram. Int.* **2015**, *41*, 79–84. [[CrossRef](#)]
45. Cullity, B.D. *Elements of X-Ray Diffraction*; Addison-Wesley Publishing Company: Boston, MA, USA, 1967.

46. Shi, L.; Sun, C.; Gao, P.; Zhou, F.; Liu, W. Mechanical properties and wear and corrosion resistance of electrodeposited Ni-Co/SiC nanocomposite coating. *Appl. Surf. Sci.* **2006**, *252*, 3591–3599. [[CrossRef](#)]
47. Beltowska-Lehman, E.; Indyka, P.; Bigos, A.; Szczerba, M.J.; Kot, M. Effect of hydrodynamic conditions of electrodeposition process on microstructure and functional properties of Ni-W/ZrO₂ nanocomposites. *J. Electroanal. Chem.* **2016**, *775*, 27–36. [[CrossRef](#)]
48. Zhang, Z.; Chen, D.L. Contribution of Orowan strengthening effect in particulate-reinforced metal matrix nanocomposites. *Mater. Sci. Eng. A* **2008**, *483*, 148–152. [[CrossRef](#)]
49. Hou, K.H.; Chen, Y.C. Preparation and wear resistance of pulse electrodeposited Ni-W/Al₂O₃ composite coatings. *Appl. Surf. Sci.* **2011**, *257*, 6340–6346. [[CrossRef](#)]
50. Amadeh, A.; Moradi, H. Wear behavior of carbon steel electrodeposited by nanocrystalline Ni-W coating. *Int. J. Iron Steel Soc. Iran* **2009**, *6*, 14–19.
51. Hou, K.H.; Ger, M.D.; Wang, L.M.; Ke, S.T. The wear behaviour of electro-codeposited Ni-SiC composites. *Wear* **2002**, *253*, 994–1003. [[CrossRef](#)]
52. Yao, Y.W. Preparation, mechanical property and wear resistance of Ni-W/Al₂O₃ composite coatings. *Surf. Eng.* **2008**, *24*, 226–229. [[CrossRef](#)]
53. Chen, X.H.; Chen, C.S.; Xiao, H.N.; Cheng, F.Q.; Zhang, G.; Yi, G.J. Corrosion behavior of carbon nanotubes–Ni composite coating. *Surf. Coat. Technol.* **2005**, *191*, 351–356. [[CrossRef](#)]



© 2019 by the authors. Licensee MDPI, Basel, Switzerland. This article is an open access article distributed under the terms and conditions of the Creative Commons Attribution (CC BY) license (<http://creativecommons.org/licenses/by/4.0/>).